the general science journal

PHYSICS OF COLD FUSION WITH THE BSM–SG ATOMIC MODELS

Stoyan Sarg - Sargoytchev

York University, Toronto, Canada*
World Institute for Scientific Exploration**

ABSTRACT OF THE ESSAY:
Advances in the field of cold fusion (LENR), in which the energy release cannot be explained by a chemical process, need a deeper understanding of the nuclear reactions and, more particularly, the possibility for overcoming the Coulomb barrier. The treatise "Basic Structures of Matter – Supergravitation Unified Theory", permits an explanation from a new point of view by using the derived three-dimensional structures of the atomic nuclei. The recently published monograph "Structural Physics of Nuclear fusion with the BSM-SG atomic models" provides a new approach in theoretical understanding of the physical process and the possibility for modification of the Coulomb barrier. The monograph offers: (1) A method for analysis of the LENR experiments using the BSM-SG atomic models, (2) A selection of isotopes suitable for a more efficient energy yield with a minimum of radioactive products (3) practical considerations for selection of the technical method and the reaction environment.

Keywords: cold fusion, LENR, Coulomb barrier, atomic nuclear structures, alpha decay

* Current employer
** Institution supporting this theoretical work
http://instituteforscientificexploration.org/

1. INTRODUCTION

According to current understanding of nuclear physics, fusion may occur only at super high temperatures in the order of a million degrees, so there are three main objections against cold fusion: the lack of strong nuclear emissions, the mystery of how the Coulomb barrier is penetrated, and the lack of strong emissions of gamma or X-rays. These objections rely on the officially accepted theoretical understanding and, more particularly, on Quantum Mechanics, which is based on the Bohr planetary model of hydrogen extrapolated to all atomic nuclei. According to this model, the nucleus is extremely small in the order of 10^{-15} m, so the Coulomb barrier at such a distance is extremely strong and can be overcome only with a very high collision momentum achievable at a temperature of a million degrees. Despite these objections, after Fleischmann and Pons announced a successful cold fusion in 1989 [1], the interest in cold fusion significantly increased. This led to creation of international forums with a data base [2], meetings and scientific journals promoting the research on cold fusion [3].

The year 2011 marked a significant advance in cold fusion this time coming from Italy. The research was pioneered by Francesco Piantelli in 1989, who observed a strange thermal effect at low temperature in a sample of nickel in hydrogen atmosphere [4]. The research was further extended for almost two decades by interuniversity program [5]. It was later continued by Sergio Focardi and Andrea Rossi [6] that led to development of a prototype of a commercial cold fusion reactor, called E-cat, patented by Rossi [7]. The successful demonstrations of the E-cat reactor in 2011 raised international attention. On September 22nd, 2011, NASA hosted a conference on cold fusion devices at its Glenn Research Center location in Cleveland, Ohio [8], where an opinion was indorsed that the cold fusion might be feasible. The current understanding of nuclear reactions could not explain cold fusion or LENR and many scientists voiced a need for a new theoretical explanation. The conclusion is that unbiased scientific discussion is highly necessary.

2. A NEW THEORETICAL APPROACH

2.1 Brief introduction

The feasibility of cold fusion was theoretically recognized by Dr. Stoyan Sarg after he developed the BSM-Supergravitation unified theory (BSM-SG) [9] and more particularly the understanding that alpha decay is a kind of cold fusion of properly oriented nuclear substructures inside the atomic nucleus [10]. After the first copyright protection in CIPO Canada in 2001 [11], the BSM-SG theory and related articles were posted in physical archives [9,11,12,13] and reported at a number of international scientific conferences. Scientific papers were published in Physics Essays [14], Journal of Theoretics [15] and conference proceedings [16,17]. The complete theory was published as a book in 2006 [18]. The BSM-SG theory is based on an alternative concept of the physical vacuum that has not been investigated before. The models developed as a result of the suggested concept are in excellent agreement with experimental results and observations in different fields of physics. The initial framework is based on two indestructible fundamental particles, FP, with parameters associated with the Planck scale and a fundamental Law of Supergravitation (SG). This law is distinguished from Newton's law of gravity in that the SG forces, F_{SG}, in pure empty space are inversely proportional to the cube of distance (while the gravitational forces in Newton's law are inversely proportional to the square of distance).

$$F_{SG} = G_0 \frac{m_{01} m_{02}}{r^3} \qquad \text{(SG Law)} \qquad (1)$$

where: G_0 – SG constant, m_{01} and m_{02} - SG masses (different from the Newtonian mass) , r - distance

The two FP particles combine in hierarchical formations of 3D fractal structures held by SG forces. In far range propagation through the space-fabric of the physical vacuum, the SG forces become gravitational forces of Newton's law of gravity. In contrast to the methods in Quantum Electrodynamics, the BSM-SG theory applies Classical Electrodynamics and the SG law. The suggested concept and derived physical models allow explanation of all kinds of quantum mechanical interactions between the unveiled substructure of the elementary particles, from one side and the space-time fabrics from the other. Since the elementary particles appear to have a 3D non-spherical structure and shape, the atomic nuclei also possess non-spherical 3D geometrical structures that define the row and column pattern of the Periodic Table. In this sense, one of the major results of the BSM-SG theory is a new vision of the 3D structure of protons and neutrons and their spatial arrangements in atomic nuclei. This is presented in the Atlas of Atomic Nuclear Structures (ANS) that was archived in the National Library of Canada [12] and published elsewhere (viXra:1107.0031).

2.2. Non-spherical shape of protons and neutrons and their spatial arrangement in atomic nuclei according to BSM-SG theory

In Quantum Mechanics (QM) and Particle Physics all particles are assumed to be spherical, so QM deals only with energy. This excludes the option that particles might have a denser non-spherical fine structure. The assumption of the spherical shape of atomic nucleus is based on the Bohr planetary model of hydrogen, despite that some of its enigmatic problems have not been solved from the time of its adoption. Based on scattering experiments in which only a spherical shape is assumed, the nucleus is considered extremely small in the order of 10^{-15} m. The main scattering experiments are two types: scattering of positrons from a positive atomic nucleus (or the proton in case of hydrogen), known as Bhabha scattering, or Rutherford scattering of alpha particles from a thin foil of gold. However, the scattering experiments have only angular, and not transverse, resolution. Then if the nucleus is assumed to be non-spherical, such as a torus, a twisted torus, or a folded torus with much larger toroidal radius but thinner, the scattering data by positrons will be one and the same. Also, the positrons as well as the electrons are found to have rotational speed, so the momentum of this will affect the interpretation of the scattering data. In the Rutherford scattering experiment, if the Helium nucleus is not spherical, the data will be influenced by a channeling effect that also will contribute to a smaller angular dispersion. (This is illustrated by Fig. 8.22 of BSM-SG book).

If the shape of protons and neutrons forming the nuclei are not small spheres, but twisted and folded torus, with the same masses, then the strong nuclear forces will be spread over a much larger distance, but still inside a volume approximately equal to the volume of a sphere with a Bohr's radius $a_0 = 0.523$ Angstroms. For the real hydrogen nucleus, this volume may not have the shape of a sphere, but an ellipsoid, while in other atomic nuclei it might have a different shape. Then in the case of hydrogen, the QM energy levels will appear exactly the same as in the Bohr model, but the strong nuclear and Coulomb forces in that particular volume will have quite a different configuration. The real physical models of atomic nuclei could be completely different from the QM models. Then the Coulomb force at the center of the atomic nucleus will not converge to a small sphere with a radius of 10^{-15} (m), but will have a much lesser strength spread in a non-spherical volume. This is exactly the case for the BSM-SG models of the atomic nuclei. Direct observations with the most powerful electron microscopes barely reach a resolution of 1 Angstroms (1x 10^{-10} m), which is still poor in comparison to the Bohr radius of hydrogen $a_0 = 0.523$ Angstroms. Despite this, some advanced electron microscope images begin to show features of a non-planetary atomic model (this will be discussed later). According to BSM-SG, the strong nuclear forces are from the SG forces defined by Eq. (1) for pure empty space. But in the space fabric of the physical vacuum (called a Cosmic Lattice in BSM-SG), for a distance smaller than the Bohr radius they may obtain a higher inverse power order of dependence on distance due to a leakage of the SG forces at closed proximity (discussed in Chapter 2, p. 2-17 of BSM-SG). The detectable signatures of the SG forces are the Casimir forces, some Van der Waal forces, and some observations in nanotechnology where single atoms put in a flat metal lattice become stick on. Other observational signatures are the clustering of the electrons in electron beams and the whole Quantum Hall effect experiments at room temperature.

The BSM-SG atomic models provide a completely new approach for investigating the Coulomb barrier. The initial guess about the shape of the proton and neutron was intuitively obtained when analyzing the data from particle physics experiments. Why do the initially obtained unstable particles from the collisions of protons and neutrons, such as pions and kaons and their decay products to muons and electrons (positrons), exhibit so consistent masses? The logical answer is that these unstable particles might be enclosed inside of a torus, so when this torus is cut in just one place, the pions and kaons are also cut in one place. But in this new shape, they are unstable and undergo further decay. One big enigma not solved for many decades (due to the adopted concept of the physical vacuum) is that the sum of the masses of the first products (pions and kaons) is larger than the proton or neutron mass. The BSM-SG analysis discovered that the kaon structure, while still helical has a different overall shape from the helical structure of other particles (pions, muons, electron, positron), so it exhibits a lower inertial mass property in comparison to them. This causes inaccuracy in the kaon mass estimation. Correcting this problem revealed the internal structure of the stable proton and neutron particles. The detailed analysis of Particle Physics data is presented in Chapter 6 of BSM-SG. Once the enigmatic problems about the shape and fine structure of the stable elementary particles (proton, neutron, electron and positron) were solved, everything from particle physics to cosmology became highly logical and understandable.

The question why the chemical and physical properties of the elements in the Periodic Table do not follow strictly the row and column pattern, has not been answered from the time of Mendeleyev. Could this be a signature of some three-dimensional composition of fractal structures from which the atomic nuclei are built? The extensive analysis of experimental data in different fields of physics led to envision the shapes of the proton and neutron that permitted to reveal their structural arrangement in the atomic nuclei in order to match the raw and column pattern of the Periodic table. The proton has the shape of a twisted torus in the form of the figure 8, while the neutron is a double folded torus. Their shapes are different three-dimensional curves, but they have one and the same superdense substructure composed of helical structures (discussed in

Chapter 6 of BSM-SG). In the BSM-SG theory, the validation of this conclusion involved extensive analysis of the Particle Physics data, and matching of the derived models with the theoretical developments of Quantum Mechanics, chemistry and experimental data from different fields of physics.

Fig. 1 illustrates the revealed shape and the spatial arrangement of the protons and neutrons in the atomic nuclei of the elements Hydrogen, Deuteron and Helium according to the BSM-SG theory.

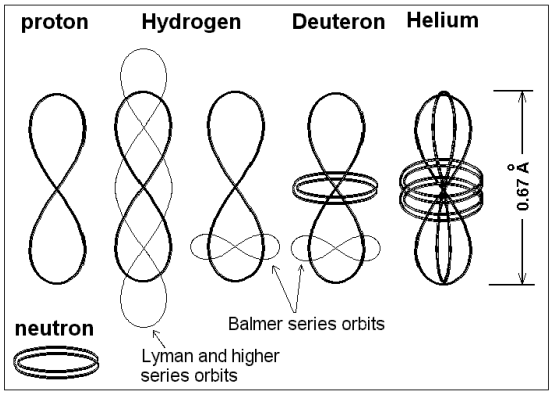

Fig. 1. Shapes of the proton and neutron and their nuclear configuration of H, D and He atoms according to the BSM-SG

Fig. 2. illustrates the cluster chain structure of atomic nuclei with Z-number larger than 18 (Argon) according to BSM-SG models.

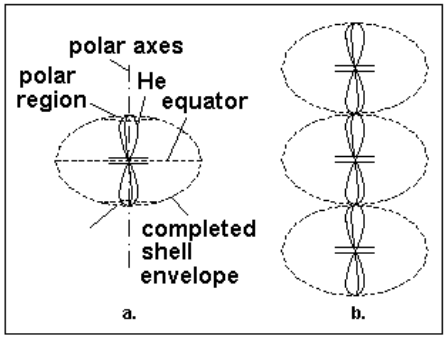

Fig. 2. a.- completed shell of Argon (the envelope is shown), b. – a chain structure in heavier elements.

When using the shape of the proton and neutron according to BSM-SG, and going through the Periodic Table by consecutive increase of the z-number, we find an extraordinarily good match to the pattern of the Periodic Table of stable isotopes. In such an approach, the physical meanings behind the Hunds rule, the Pauli exclusion principle, the shell completion, valences, oxidation numbers, first ionization potential and X-ray properties are revealed. Additional new features of the nuclei are also revealed, putting a new light on the physics of the nuclear bonds, the completion of the shells and what defines the valences and the direction of the chemical bonds. These features are discussed in detail in Chapter 8 of BSM-SG. The revealed physical configurations of the atomic nuclei of all stable isotopes up to z = 103 (Lawrencium) are presented in the BSM-SG Appendix Atlas of Atomic Nuclear Structures (ANS), one of the major derivatives of BSM-SG, also published separately [12]. Figure 2 shows a graphical view of some selected atomic nuclei as derived in BSM-SG theory and included in the Atlas of Atomic Nuclear Structures [12].

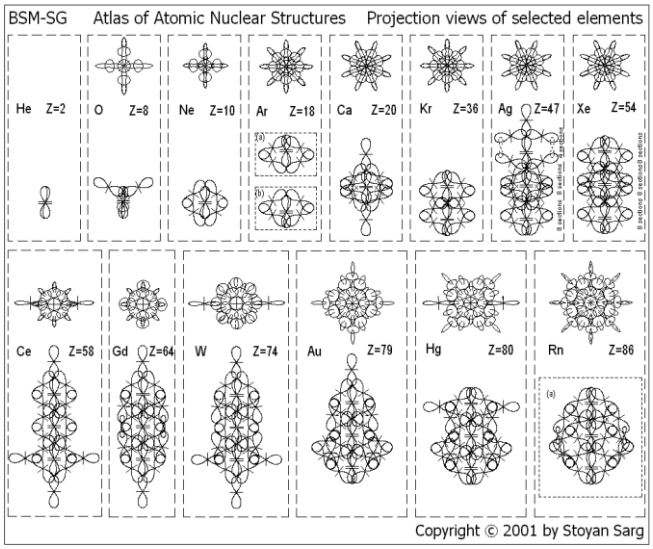

Fig. 3. Extract from the Atlas of the Nuclear Structures showing the graphical view of the atomic nuclei of some elements [12]

From Fig. 3 we see that the nuclear overall shape for elements with 18<Z<86 have not spherical but elongated shape. The protons (deuterons) in the completed shells have strong nuclear bonds GBclp and weaker EB bonds. (§8.3.6, Chapter 8 of BSM-SG). The element Ag has both types of bonds (see also Fig. 15). GBclp bonds are more compact and exhibit a full polar axis symmetry of the near Coulomb field. The EB bonds, responsible for secondary valences have more extended Coulomb field and may not be fully symmetrical. They tend to get symmetrical

with the increase of Z-number until converted to GBclp bonds, which are fully excluded from valences (see Fig. 15 discussed later). The symmetrical arrangement of the Coulomb field plays an important role for the atomic arrangement in the metal lattice. They keep the orientation of neighboring atoms. The detectable signature of this orientation are the Laue patterns obtained by the X-rays spectroscopy. High-resolution images from electron microscopy also confirm this.

The Russian professor Dr. Kanarev, a theorist and cold fusion researcher [19], also arrived at the idea that the atomic nuclei are not blobs of protons and neutrons but have a 3D spatial arrangement [20]. However the protons and neutrons of Kanarev's models are spherical and their spatial arrangement is quite different.

2.3 Coulomb barrier of the proton

According to BSM-SG theory, the SG forces are not only behind the nuclear forces. They also define the field lines of the electrical charge in close proximity to the proton core. Therefore the SG field also defines the so-called Coulomb barrier that is one of the most controversial issues in nuclear fusion. Fig. 4 illustrates the distribution of the electrical field (E-field) in close proximity to the proton's high-density core and the locked E-field around the neutron's high-density core. The E-field of the neutron is locked in proximity due to the strong SG forces that curves the electrical field the energy of which is supplied by the SG field.

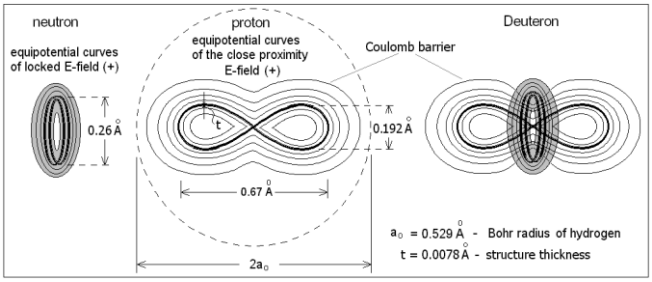

Fig. 4. Graphical illustration of the Coulomb barriers of the proximity E-field of the proton and the locked E-field of neutron. Both, the proton and neutron create the E-field as a modulation of the physical vacuum (CL space) by their superfine substructures made of helical structures. The E-field of the neutron is locked in the near field surrounding its shape.

The core internal structure of the proton and neutron has the features of a spring, since they both are composed of helical structures with distributed E-field and SG field. In fact the electrical charge is caused by modulation of the physical vacuum by the strong SG forces of the superdense helical structures. The electrical charge in close proximity to the proton is distributed around its shape, but this is in a microscopic range smaller than the Bohr radius and its shape could not be detected by existing technology. Outside of the Bohr radius, the E-field lines of the proton appear as coming from a point charge. The neutron has the same internal structure, but a different shape that causes the charge to be locked in proximity. The signature of its locked electrical charge appears only when the neutron is in motion. Then it exhibits a magnetic moment that is an enigma in Modern Physics. The spatial configuration of the proton's Coulomb barrier illustrated in Fig. 4 is significantly different from the Coulomb barrier of the Bohr model of hydrogen. Furthermore it could be modified to some extent by some external SG forces from other atomic nuclei.

It is well known that a single neutron is not stable and converts to a proton with a lifetime of 12 min. The instability is caused by the weak balance between the repulsive E-field forces in the locked E-field and the attractive SG forces that keep its shape of a double folded torus. However, when the neutron is over the proton saddle (central section) it is stable, forming in such way the stable element Deuteron. The stability is a result of a balance between the repulsive E-fields (+) of the proton and the locked, but accessible at such a distance, E-field (+) of the neutron. This is graphically illustrated on the right side of Fig. 4. The neutron can only rotate or vibrate. The vibrational motion is behind a physical phenomenon known as the Giant resonance. This phenomenon, discovered by Baldwin and Klaiber in 1947, was later confirmed by many and interpreted by Goldhaber and Teller (Phys. Rev. **74**, 1046, (1948)). It was based on the assumption that the protons in the nucleus move in one direction while the neutrons move in the opposite direction. The rotational motion of the neutron contributes to the phenomenon known as a nuclear spin, since the locked electrical charge provides a magnetic field when the neutron rotates. When two neutrons are over the saddle point of a proton,

the obtained nuclear structure is Tritium. The bonding energy of this three-body system is not as strong as for Deuteron, because the two neutrons are separated by a gap due to repulsion by their locked E-fields (+) so they are away from the E-field valley of the proton. When the Tritium nucleus is included in the heavier atomic nuclei, however, it is stable because the combined E-field from other protons modifies the Coulomb field of the host proton of Tritium.

In accordance with the BSM-SG model, the process known as electron capture ($p + e^- \rightarrow n$) is just a folding of the twisted shape of the proton until it obtains the shape of the neutron as a double twisted torus, held in this shape by the SG forces. Then the charge in the far field is emitted as a Beta particle. The latter is a high-energy virtual particle, which is distinguished from the low energy real positron. The "electron capture" happens in some nuclear reactions and especially in the radioactive decay of the fission chain reactions leading to unstable nuclei. The BSM-SG model also provides an answer to the long-standing problem of the "missing neutrino" from the Sun. The mass difference due to the slight shrink of the spring-like structure of the neutron in the conversion of the proton to a neutron is wrongly attributed to the emission of a neutrino particle. Neutrino particles detected in some experiments are fractions of broken substructures from elementary particles.

From the graphical model of the Coulomb barriers in Fig. 4 it is evident that a nuclear reaction $p + d \rightarrow D$ would take place if the neutron and protons are properly oriented and the proton's Coulomb barrier is slightly modified. Technical methods for this possibility will be discussed.

2.4. Evidence for some features of the BSM-SG atomic models from some high-resolution electron microscope images

The E-field lines outside of the boundary defined by the Bohr radius (for hydrogen) will appear as coming from a point charge. Electron microscopes, for theoretical and practical reasons, cannot sense the region inside of this boundary. However they may detect some non-uniformity of a single sheet lattice that is not explainable by Quantum Mechanical models of atoms. Such example is an electron microscope image of the single sheet structure of grapheme, as shown in Fig. 5.a. Panel a. shows the published original image of grapheme [21], while Panel b. shows the same image with adjusted brightness in order to fit the scale of display. Fig. 5.c shows the sketch of the carbon nucleus according to BSM-SG. The protons p_3 and p_4 are in the drawing plane, while the protons p_1 and p_2 (shown smaller) are in a plane perpendicular to the sheet.

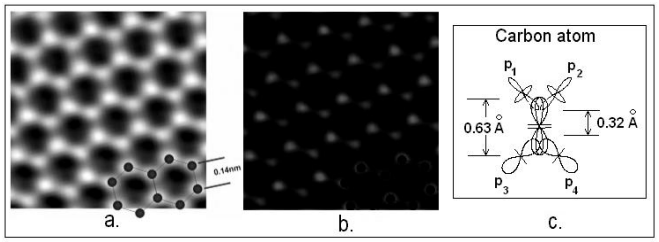

Fig. 5. a. Single wall Carbon sheet with TEAM microscope [21]; b. Processed image by brightness adjustment; c. Sketch of the carbon nucleus (p_3 and p_4 lie on a drawing plane, p_1, and p_2 are perpendicular to the drawing plane)

According to QM models the connecting bonds of carbon should lie in one plane, but according to the BSM-SG model, they do not. This means that the electron microscope image of a single sheet of carbon atoms will show a brightness difference of every neighboring bond that in fact is what is detected by the electron microscopy. If using the 3D model of carbon, shown in Fig. 5.c, we understand why the detectable neighboring bonds show a brightness difference.

2.5. Radioactive alpha decay in the heavier elements as a cold fusion of deuterons

Since the protons in the atomic nuclei are in a closer range than the space defined by the proximity E-field of the free proton shown in Fig. 4, their Coulomb barrier is distorted. This means that in the heavier atoms a spontaneous fusion between deuterons might take place with some probability. This happens naturally in the heavier atomic nuclei with $Z > 57$ (beginning from the Lanthanides) and the process is known as a radioactive alpha decay. Fig. 6 illustrates graphically the decay process in Gadolinium [10] (archived in NLC, Canada (2002).

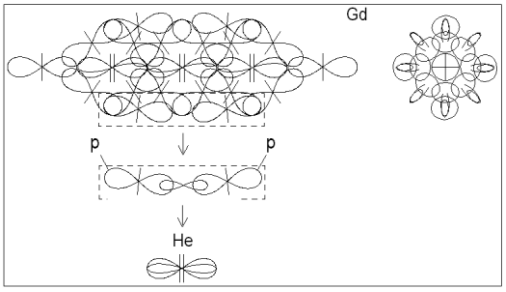

Fig. 6. Alpha decay of Gd. The two deuterons are shown prior to their fusion into helium nucleus.

The fusion of the two deuterons into He in alpha decay is a transition process. Since it happens in room temperature we may conclude that cold fusion at room temperature is possible under special conditions.

2.6. How the valence protons (deuterons) of the atomic nuclei define the direction of chemical bonds in agreement with the VSEPR models in chemistry.

The BSM-SG atomic models also have other important features. The nucleus of every element has a well-defined rotational symmetry around an axis that we may call a polar axis. Another feature is that every atomic nucleus with a Z-number larger than one has at least one helium nucleus in the middle of its nuclear structure because helium nucleus is the densest one. The heavier atomic nuclei have more than one He nucleus and they are aligned with the polar axis as a chain (see Fig. 1 b.). Most of the protons and neutrons are combined in deuteron nuclei but some single protons also exist in the nuclei. In atomic nuclei with z > 2 and especially the heavier elements, tritium nuclei may also be included in some isotopes but the embedded tritium is stable. The internal nuclear shells are tightly bound by the SG forces and do not participate in chemical reactions, but the deuterons or protons from the external shells with their electrons are involved the chemical valences. One important feature of the valence protons (deuterons) from the external shell is that one end is bound to the polar spot by SG forces, while the other end has a limited angular freedom in a plane passing through the polar axis. However, they have a tight angular restriction in any perpendicular plane. The angular positions of the valence protons (deuterons), combined with the 3D geometrical shape of the nuclei, define the angular positions of the chemical bonds. Another important feature of revealed atomic structures is that the electrons do not form arbitrary clouds. They move in individual quantum electron orbits whose positions and traces are defined by the close proximity electrical field of the proton, so they are bound to the protons. The quantum orbits are in a strong SG field with a non-linear gradient, so the orbits for the different energy levels are quite close. Since valence protons (deuterons) have an angular freedom in a plane passing through the polar axis, protons from the opposite poles of a single chain element sharing one and the same restricted meridian section become connected by one quantum orbit, so they are excluded from the principle valence. All these features of the atomic nuclei are clearly evident from the atlas of ANS, if following the trend of Z-number through the periodic table. Fig. 7 illustrates two rows of the Periodic Table. The protons and deuterons from the external shell defining the chemical valence are clearly distinguishable.

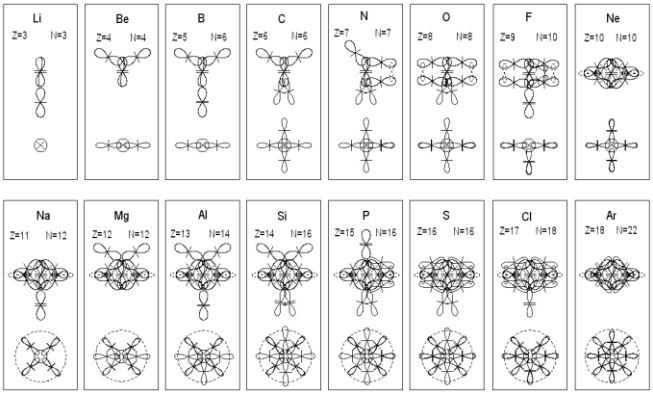

Fig. 7. Atomic nuclei from two columns of the Periodic Table

2.7. Why the nuclear chain reaction induced by slow neutrons leads to many radioactive products.

For all stable isotopes the increase in the number of neutrons is faster than the Z-number (protons) increase. This enigma is not explainable by QM models of atomic nuclei. BSM-SG models provide an explanation based on the discovered problem referenced as a “polar region problem” in atomic nuclei (§8.3.7, Chapter 8 of BSM-SG). It is caused by the closer accumulation of proximity E-fields from the protons at the polar region of atomic nucleus when the Z-number increases.

According to BSM-SG this is naturally compensated by accumulation of more neutrons in the equatorial region. This modifies the E-fields in the polar regions (due to SG forces) making the isotopes more stable. The excess neutrons are bound to the protons as deuterons and tritium nuclei. However this trend must match the rotational symmetry of atomic nuclei. It has some relation to the nuclear spin number and it is important for stability. As a result some elements have more than one stable isotope, while others do not. Technetium, for example, is an element that does not have a stable isotope. Examining the Z-trend increase in the Atlas of ANS we may see that the spatial arrangement of the protons (deuteron, tritium) in the stable isotopes has a good symmetry in respect to the polar axis.

It is well known that the nuclear chain reaction requires slow neutrons. The slow neutrons are embedded for a short time in the recipient nuclei. They make them unstable and they decay to other unstable nuclei. Having in mind that the positions of the neutrons in the stable isotopes are highly symmetrical in respect to the polar axis, there is a very low probability that the captured neutron will be in the right place. That's why the nuclear chain reaction provides a lot of radioactive byproducts with different decay times, but most being very short. This is in sharp contrast to cold fusion where radioactive byproducts are very rare or absent. All presently existing nuclear power plants are based on nuclear fission chain reactions that are responsible for accumulation of a large quantity of radioactive waste.

2.8. Unit charge. Structure of the electron and trace lengths of the quantum orbits

Quantum Mechanics cannot provide answer about the enigma: why do the proton, electron and other elementary particles with different masses have one and the same unit electrical charge? Such explanation is suggested in BSM-SG §2.15.2, Chapter 2 of BSM-SG. The charge is not a substance contained inside of the particle, but a kind of modulation of the CL space (physical vacuum) by the SG field of the helical sub-substructure of the particle. Since the overall shape of the stable particles is defined by the SG field balance in the CL space, particles with different masses appear to have one and the same unit charge.

The Quantum orbits in the BSM-SG models of atoms are derived by the unveiled material structure of the electron presented in Chapter 3 of BSM-SG and published in the peer review journal Physics Essays [14]. The revealed shape of the electron is a cut torus having a small helical step, while it also possesses a fine material structure made of helical structures. The external helical structure modulates the CL space (physical vacuum) by creating a negative electrical charge. The electron and its fine helical structure according to BSM-SG are graphically illustrated in Fig. 8, where R_c - is the Compton's radius, s_e – is the helical step of cut torus.

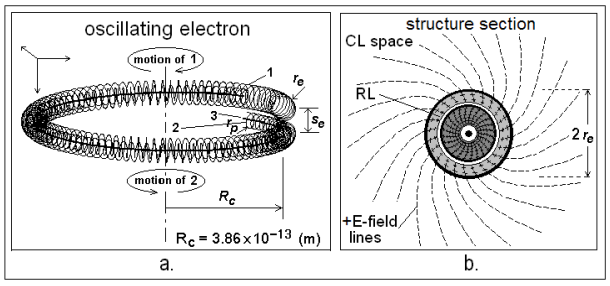

Fig. 8. Structure of the electron according to BSM-SG

The electron is a 3-body system, exhibiting rich oscillation properties. When interacting with the CL structure of the physical vacuum, this model exhibits all known QM properties of the electron. Let us suppose that the structure of the electron moves as a screw, so that the peripheral velocity is equal to the speed of light and it makes one revolution for a Compton time. The axial velocity is

$$\upsilon = \frac{cs_e}{\sqrt{4\pi^2 R^2 + s_e^{\,2}}} \qquad (2)$$

Let us assume that this quite specific screw type of motion corresponds to the electron motion in the Bohr atom at orbit a_0 with energy of 13.6 eV (a proof shown in [14] and Chapter 3 of BSM-SG). Then the axial velocity is

$$\upsilon = \frac{e^2}{2h\varepsilon_0} = \alpha c = 2.18769\times10^6 \quad (m/s) \qquad (3)$$

where: e – charge of electron, h – Planck constant, c –speed of light, α - fine structure constant

$$2\pi R_c = \lambda_C = c/\nu_C \qquad (4)$$

Solving (2) and (3) and substituting (4) we obtain the helical step s_e

$$s_e = \frac{\alpha c}{\nu_c\sqrt{1-\alpha^2}} = 1.77\times10^{-14}\ (m) \qquad (5)$$

where: $\nu_c = 1.2356\times10^{20}$ (Hz) - Compton frequency, λ_c - Compton wavelength

It is known that the electron possesses a magnetic moment anomaly whose theoretical value is $0.5\alpha/\pi$, but its physical explanation has been an enigma so far. According to Eq. (5) the anomalous magnetic moment is due to the helical step, so the fine structure constant appears embedded in the structure of the electron.

At the same time when the electron performs a screw-like motion with axial velocity αc corresponding to 13.6 eV, the structure of electron oscillates with its first proper frequency equal to the Compton frequency. This is an optimal quantum velocity, according to BSM-SG, in which the phase of the oscillating electron matches the phase of the SPM vector (Spatial Precession Momentum) – a characteristic feature of the Cosmic Lattice node, which exhibits spatial oscillations with a Compton frequency (§2.9, Chapter 2 of BSM-SG). The phase propagation of the SPM vector in CL space (physical vacuum) is behind the constancy of the speed of light. The screw-type oscillating motion of the electron, referred to as confined motion, defines preferred quantum velocities, which appear as energy levels in the hydrogen atom. Consequently, the principal quantum numbers of the Bohr model of hydrogen are in fact signatures of the motional behavior of the electron structure in the fabrics of the physical vacuum [14].

From the confined motion of the electron, a quantum efficiency factor is directly derivable (§3.11.A.1, Chapter 3 of BSM-SG).

$$\eta = (1-v^2/c^2)^{1/2} \qquad (6)$$

Its inverse value is the relativistic gamma factor. For velocities larger than αc, the electron rotation is slower, so the tangential velocity never exceeds the speed of light. Then the inverse factor η becomes the relativistic gamma factor. The quantum interactions with the CL space make the motion with higher velocities more difficult, which explains the relativistic mass increase predicted by Einstein.

When the electron moves in a closed trajectory, the phase match between the SPM frequency of the CL structure (physical vacuum) and the two proper frequencies of the electron defines two important parameters of the quantum orbit: its trace length and the duration (a lifetime of the excited state) [14]. Therefore, the quantum orbits have different trace lengths for different quantum velocities of the electron. This is valid also for the quantum orbits in molecules serving as chemical bonds for molecules that exhibit vibrational-rotational spectra.

In §7.8.2 Chapter 7 of BSM-SG, the Balmer model series of hydrogen is derived based on the BSM-SG model in which the strong SG field is involved. The calculated energy levels match the energy levels of the Bohr model of hydrogen. Another important feature is that the electron orbits in the BSM-SG model of hydrogen are much more closely packed in comparison to the Bohr model. This is because, according to Newton's second law, the radius of the electron orbital motion in a circular trajectory (in Bohr model) is inversely proportional to the square of velocity, while in the BSM-SG model it is inversely proportional to the velocity (considering the SG field and SG masses). However, because of fast attenuation of SG forces with the distance, the length of the quantum orbit for 13.6 eV in the BSM-SG model is equal to the length of the Bohr orbit defined by the Bohr radius $a_0 = 0.52918$ Angstroms. The shape of the orbit, however, is not circular but follows the equipotential curve of the close proximity E-field of the proton. This explains the p-shapes of the wave functions observed in hydrogen, a feature that cannot not be explained by the Bohr planetary model using the classical electrodynamics. Two distinctive positions of the quantum orbits in hydrogen corresponding to the Lyman and Balmer series are shown in Fig. 1.

During the finite lifetime of the electron in a particular quantum orbit, it modulates the CL space that increases the local energy and, when dropping to a lower quantum orbit (lower energy level), this energy is released as a photon. This explains what is behind the Heisenberg

Uncertainty Principle in Quantum Mechanics – the photon energy is not emitted directly from the electron, but from the space fabric containing the pumped energy from many orbital cycles.

In the internal shell of the heavier atoms, the strong SG field also contributes to the energy levels.

The interaction of the electron in its optimal confined motion with the Zeropoint energy provides a constant driving momentum. In the case of Rydberg atom this momentum drives the atomic nuclei and the magnetic moment of the electron interacts with the magnetic moment of the nucleus at proper nuclear spin state. This effect discussed in details in [24] might favor the process of a nuclear fusion between the hydrogen (deuterium) and the nucleus of a proper selected element (isotope).

2.9. Configuration of simple molecules

Fig. 9 a. and b. show two states of the hydrogen molecule H_2. In the state shown in a. and referred to as an ortho-state, the two protons are connected by a single quantum orbit with two electrons counter-circling in the orbit. In the other state of H_2 shown in b. the two protons are connected by two separate orbits.

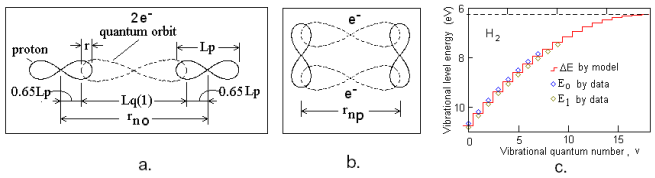

Fig. 9. a. – shape of H_2 molecule ortho-state, b. shape of H_2 molecule para-state, c.- energy levels by the BSM-SG model for ortho-state H_2 molecule and its match to experimental data

The parameters of the ortho-state H_2 molecule (shown in Fig. 9.a) were obtained in §9.6 of BSM-SG by analysis of the photoelectron [22] and optical [23] spectra. Using the total energy balance in which SG field energy is included, the expression (7) is derived (§9.7 of BSM-SG) providing the vibrational energy levels. This expression involves the total SG energy balance that includes the SG attraction, the kinetic energy of the electron E_k, the energy of the proton charge E_q, and the molecular binding energy. The vibrational energy E_V is plotted in Fig. 9.c together with the energy levels corresponding to the identified corresponding optical spectrum band of the H_2 molecule. The calculated energy levels are in excellent agreement with the experimental data.

$$E_V = \frac{C_{SG}}{e[[L_q(1)(1-\alpha^4\pi\Delta^2)]+0.6455L_p]^2} - \frac{2E_q}{e} - \frac{2E_k}{e} + E_B \quad (7)$$

$$C_{SG} = G_0 m_0{}^2 = (2h\nu_c + h\nu_c\alpha^2)(L_q(1)+0.6455L_p)^2 \quad (8)$$

$$C_{SG} = 5.2651\times10^{-33} \quad \left[N\,m^3\right] \quad (9)$$

where: e – unit charge, $L_q(1) = 2\pi a_0 = 3.325\,\overset{0}{\text{A}}$ – quantum orbit length for electron velocity of 13.6 eV, $L_p = 0.667\,\overset{0}{\text{A}}$ – proton length, E_q = 511 KeV – unite charge energy, E_k – electron kinetic energy, ν_c – Compton frequency, α - fine structure constant, G_{SG} – SG constant, m_0 – SG mass of the proton (also neutron), $E_B = 6.26\,eV$ - energy difference between the dissociated limit and the metastable state, $\Delta = (V_L - x)$ - vibration level (V_L – plotting vector origin, x – argument)

The para-state of the H_2 molecule is more compact so it is more stable against collisions from Brownian motion.

The analysis of H_2 and D_2 molecules permitted the derivation of one important physical parameter of the SG law denoted as C_{SG} (Eq. 8). The obtained value of C_{SG} is additionally verified in §6.14.1, Chapter 6 of BSM-SG, where it was used for theoretical calculation of the binding energy of the proton and neutron in the Deuteron. The estimate is based on a classical approach similar to calculation of the Newtonian gravitational potential but using the SG law instead. The applied approximate method is illustrated in Fig. 10.

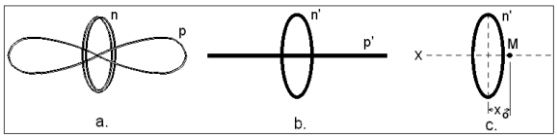

Fig. 10. Approximate method for verification of C_{SG} parameter**. a.** The nucleus of Deuteron, **b.** – an equivalent model where the neutron SG mass is presented as a mass ring and the proton SG mass as a mass bar., **c.** – additional simplification by presenting the SG mass bar as a SG mass point.

The binding energy is equal to the disintegration energy when separating the neutron from proton along the axis of symmetry *x*, while using the SG law defined by Eq. (1). The equation

(10) derived in §6.14.1, Chapter 6 of BSM-SG provides approximate value for theoretical estimation of the binding energy based on the above mentioned approach for $x_o = 0.07377$ angstroms and using a factor 2 (for some shape factor correction).

$$E_{SG-bind} = \frac{2\alpha C_{SG}}{(x_0^2 + r^2)e} = 2.158 \times 10^6 \ (eV) \qquad (10)$$

The obtained value distinguishes from the experimental value of binding energy 2.22457x10^6 (eV) only by 3%.

Fig. 11 shows configurations of some simple molecules, where the internuclear distances are estimated in Chapter 9 of BSM-SG by using the factor C_{SG}.

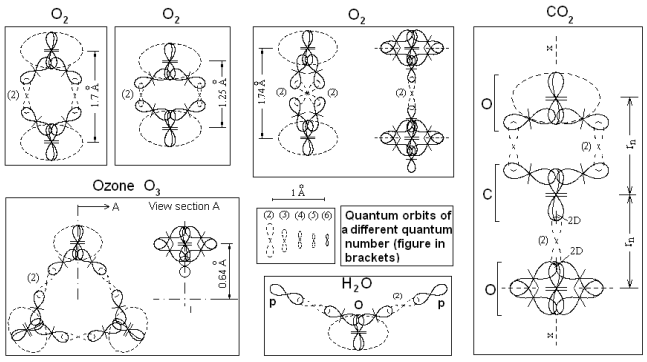

Fig. 11. Configuration of simple molecules using BSM-SG models

The derived parameter C_{SG} appears to be quite useful for approximate estimation of the distance between a proton (deuteron) and the center of mass of a recipient atomic nucleus in a process of a nuclear transmutation or cold fusion. The method for such estimate is presented in the book "Structural physics of cold fusion with BSM-SG atomic models" [24].

2.10. General Relativity (GR) from the point of view of BSM-SG theory and a hypothesis of GR field micro-curvature around the atomic nuclei.

According to General Relativity (GR), a massive object creates a field curvature (the space is shrunk). The radial dependence of this shrinkage is asymptotically smooth. Let us consider two spherical zones with finite thickness centered on the massive object and denote them as near and far zones. The photon emitter or the observed event could be in the near zone and the observer in the far zone or vice versa. Now we need to find an etalon for unit distance. It must be some characteristic parameter available in both zones. In the optimal confined motion of the electron with energy of 13.6 eV for one full turn, its cycle matches the phase of the external SPM cycle and the trace length of the curve is equal to the Compton wavelength $\lambda_C = 2\pi R_C$. So the Compton wavelength is equal to the SPM wavelength and this equivalence should be valid for both the near and far zones of the space curvature. Since the Compton wavelength is directly related to the Plank constant h by the expression $E = hc/\lambda$, it could be considered as a unit length etalon for measuring the energy of the emitted photon that passes between the two zones.

In the near zone the Compton wavelength etalon will be shorter than in the far zone. Then the wavelength of the photon emitted in the near zone but detected in the far zone will be gradually expanded, so it will exhibit a red shift. The wavelength expansion will be valid for the entire EM spectrum range since the photon wavelength is a whole number of Compton wavelengths. This explains the gravitational red shift of the photons generated near the Sun and observed at the Earth. From this explanation we may formulate one important conclusion:

The field curvature of space (physical vacuum) possesses the property of conserving energy.

2.10.1. Field microcurvature around atomic nucleus

If the field curvature, according to General Relativity, does not have a limit, we may assume that such an effect may exist also in around the nucleus due to accumulation of the superdense structures of the elementary particles. In fact, a detectable signature of field curvature in close proximity to atomic nuclei exists. This is the experimentally measured Lamb shift corresponding to the transition $2S_{1/2} - 2P_{1/2}$. It is in contradiction to the Dirac definition that these two energy levels must be the same, and in QED it is often attributed to the finite size of the atomic nuclei and vacuum polarization. The Lamb shift, first discovered for hydrogen by Lamb and Rutherford in 1947, was investigated and

measured for elements with Z>2, which are ions with only one electron. According to the Coulomb law, if the single electron is in such a strong field, the potential should increase linearly with Z-number. The observations, however, show that the Lamb shift increases with Z-number somewhat steeper than Z^3. Fig. 12 shows the Lamb shift dependence on Z-number for the elements from hydrogen to zinc. The data are from the article by Glen W. Erickson [25] recommended by NIST.

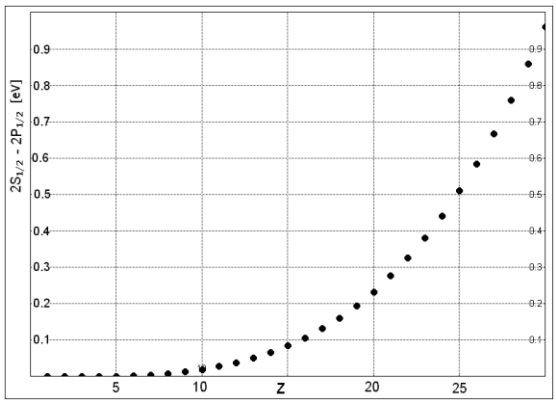

Fig. 12 Lamb shift as a function of Z-number

Fig. 12. shows that the Lamb shift dependence on Z– number is smooth, but its dependence on the mass number (protons + neutrons) shown in Fig. 13 is not smooth.

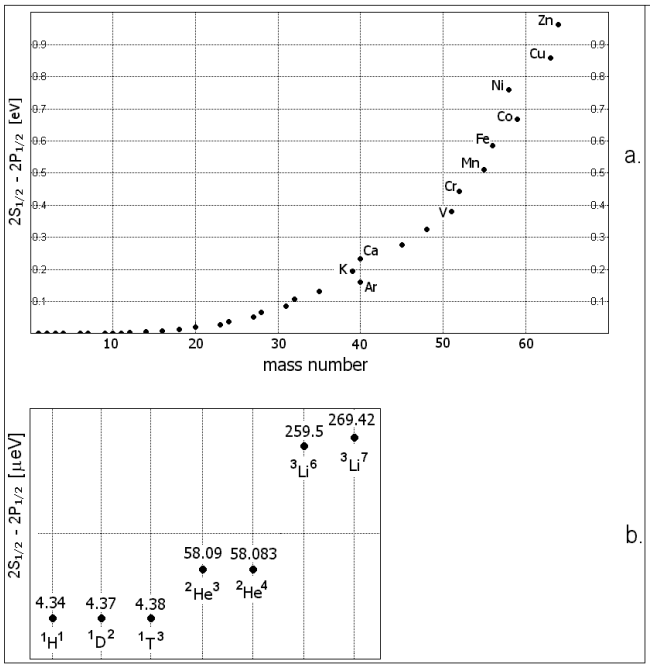

Fig. 13. a. - Lamb shift as a function of mass number, **b**. – Lamb shift for the first few elements

From Fig. 13 we see that there is an anomaly, as shown for K, Ar and Ca. This anomaly is consistent with the change in the K-edge level of the X-ray mass attenuation coefficient discussed in §8.4.1, Chapter 8 of BSM-SG. In fig 11.c we see that the changes in Lamb shift from $^1H^1$ to $^1D^2$ to $^1T^3$ are insignificant, but the change at $^2He^3$, where the two protons fuse into a He nucleus (see Fig 1) is significant. Then the Lamb shift slightly decreases at $^2He^4$ from the added second neutron over the two protons. The jump of Lamb shift at $^3Li^6$ indicates the addition of a new proton at the polar region. Then it slightly increases after a neutron is added over that proton in $^3Li^7$.

For higher Z-numbers, the accumulation of neutrons also contributes to the increase in the Lamb shift but less than the protons. These signatures together with many others discussed in Chapter 8 of BSM-SG lead to the following conclusions:

(1) The quantum orbits are bound to the individual protons,
(2) The neutron is over the proton saddle. Their accumulation also reduces somewhat the strong Coulomb field near the polar regions,
(3) The SG field of the protons and neutrons contribute to the energy levels by making the space non-linear.
(4) The strong symmetry in respect to polar axis is one of the factors that defines the nuclear stability, so the most stable isotopes (especially in the lighter elements) contain even numbers of deuterons.

In QED the Lamb shift is explained by a finite nuclear size and vacuum polarization and fluctuation. The latter two phenomena are not clearly defined in Modern Physics, but if the physical vacuum contains some type of medium, the field curvature and all other phenomena of GR are logically explainable. Albert Einstein arrived at this conclusion after he developed General Relativity. In his book *Sidelights on Relativity, page 23* he writes: *To deny Ether is ultimately to assume the empty space is not (with) physical quality. ...According to the General Relativity, space is embodied with physical quality. In this sense, therefore, there exists Ether. According to General Relativity, space without Ether is unthinkable*. [26].

Consequently, we may suggest that in close proximity to a nucleus, a field micro-curvature exists as a GR effect in a microscale range.

2.11. The hidden energy of the physical vacuum as a primary source of the nuclear energy

It is known that the nuclear mass of an element is always smaller than the sum of the masses of protons and neutrons in the atomic nucleus. Such a mass difference, known as mass deficiency or binding energy, is estimated by the Einstein equation $E=mc^2$. The binding energy rises faster at low Z - numbers (especially at He^4) reaching a smooth maximum at Fe and then slowly decreases. The BSM-SG theory provides an explanation for this enigma. The nuclear shapes for elements with lower z – numbers is closer to sphere, while for larger z – numbers they become extended, as shown in Fig. 2 and 3. For this reason the SG forces make a more compact field curvature for lower z – number up to the element Fe.

A number of observations in Cosmology, such as the flattened rotation curves of the galaxies and the increasing slope of the Hubble plot at large cosmological red-shifts contradict the Big Bang model. In order to solve these problems, a number of theorists suggested the existence of dark energy. According to BSM-SG, the dark energy is a hidden energy existing everywhere in the observable Universe. However, it is not of EM type, but associated with Newton's mass according to the Einstein equation $E = mc^2$. We may estimate this energy by using the revealed material structure of the electron. Using the Einstein equation for the mass of an electron, we obtain

$$E = m_e c^2 = h\nu_c, \quad \text{then} \quad m_e = \frac{h}{c^2}\nu_c \quad (11)$$

where; m_e – mass of electron, h – Planck constant, ν_c - Compton frequency.

Expressing the m, h, c and ν_c in Eq. (11) by their dimensions in the SI system we get

$$kg = \frac{Nms}{m^2/s^2}\frac{1}{s} \quad (12)$$

Multiplying Eq. (12) by m^2/m^2 (m – dimension of length) and rearranging we obtain

$$kg = \left(\frac{N}{m^2}\right)\left(\frac{1}{m^2/s^2}\right) m^3 \quad (13)$$

The first term on the right side of Eq. (13) is a dimension for pressure, the second is for speed of light (unchanged) and the third one is for volume. Replacing the dimensions by corresponding physical parameters we obtain

$$m_e = \frac{P_S}{c^2}V_e \quad \text{(kg)} \quad (14)$$

P_S is a kind of static pressure. Since the speed of light is constant we may regard the term P_S/c^2 as a kind of normalized pressure that the space fabric of the physical vacuum exercises on the impenetrable internal volume of the electron. We may estimate it by using the volume V_e of the structure of the electron shown in Fig. 8. It can be expressed as a volume of a torus with a large radius R_c and a small radius r_e. We see that in order to oscillate the ratio between the helical step s_e and the radius r_e should be no less than 2. The dimensionless parameter known as the g-factor of the electron determines the electron spin frequency equal to $0.5g\nu_c$ for a free electron in a magnetic field. The g factor is experimentally measured with a high precision $g = 2.002319304$. Its association with the structure of the electron leads to the conclusion that the g-factor is the helical step s_e. This allows us to obtain the small radius $r_e = s_e/g$. Then taking into account that $2\pi R_C = \lambda_C = c/\nu_c$ and s_e given by Eq. (2), the volume of the electron structure is

$$V_e = 2\pi^2 R_C r_e^2 = \frac{\pi\alpha^2\lambda_C^3}{g^2(1-\alpha^2)} = 5.96\times10^{-40} \quad (m^3) \quad (15)$$

Solving Eq. (14) for P_S and substituting m_e by Eq. (11) and V_e by expression (15) we obtain

$$P_S = \frac{g^2ch(1-\alpha^2)}{\pi\alpha^2\lambda_C^4} = \frac{g^2h\nu_c^4(1-\alpha^2)}{\pi\alpha^2c^3} = 1.37358\times10^{26}\left[\frac{N}{m^2}\right] \quad (16)$$

Using the Einstein equation $E=mc^2$ and substituting m by m_e from by Eq. (14) we obtain

$$E = P_S V_e \quad (17)$$

If the volume V_e is regarded as a reference space volume, the product of static pressure and this volume $P_S V_e$ could also be regarded as a parameter of the physical vacuum. Therefore, according to Eq. (17), this product expresses the energy of the physical vacuum contained in a reference volume $V_e = 5.96\times10^{-40}(m^3)$.

$$E = P_S V_e = 8.187\times10^{-14} \quad (J) \quad (18)$$

Expressing this energy for a unit volume of 1 cm^3 we obtain

$$E_S = 1.3736 \times 10^{20} \left[J/cm^3 \right] \equiv 3.18 \times 10^{13} \ KWH \quad (19)$$

The energy expressed by Eq. (19) is the static energy of the physical vacuum, scaled to a volume of one cubic cm. It looks extremely high but this is because the enormous static pressure P_S is exercised on the extremely small impenetrable volume that the electron and other elementary particles possess. The inter-node distance of the Cosmic Lattice is on the order of $1 \times 10^{-20} \ (m)$ but the internal lattice of the electron illustrated in Fig. 8 is denser so it is impenetrable. All non-virtual elementary particles contained in the atomic nucleus possess such a dense lattice. Although the Cosmic Lattice penetrates freely through every body, it does not enter into that denser lattice of the elementary particles. Therefore, we cannot detect directly the static pressure P_S. We only feel the effect of acceleration for which the Cosmic Lattice is responsible (this is discussed in Chapter 10 of BSM-SG). So according to BSM-SG theory, the static energy E_S is a hidden energy of the physical vacuum that is directly related to the mass of the elementary particles according to Einstein equation $E = mc^2$.

Consequently, every cubic cm of the physical vacuum space contains a hidden energy of 1.3736×10^{20} (J) equivalent to 3.18×10^{13} (KWH). This, in fact, is the primary source of nuclear energy accessible by the nuclear reactions.

2.12. Access to the hidden space energy by nuclear reaction – an explanation by a General Relativistic effect in the microscale range

According to BSM-SG all stable elementary particles have impenetrable volumes of helical structures like the electron. Any stable particle with a larger mass has a larger quantity of such volume in which the electron structure is a fractal element. Then **Eq. (14) may serve as a mass equation**. It can be extended to any non-virtual particle by using the volume ratio between that particle and the electron, which is equal to the ratio of their masses. The mass equation is further extended to the nuclear mass of any element given the number of the nucleons (protons and neutrons). In this case it is better to use the ratio between the electron and neutron instead of the proton, since the normal atomic nucleus is neutral. Then the mass of any nucleus can be expressed by Eq. (20)

$$m = \frac{g^2 ch(1-\alpha^2)}{\pi \alpha^2 \lambda_C^{\ 4}} \frac{pm_p + nm_n}{m_e} \quad (kg) \qquad (20)$$

where: m_p and m_n – the mass of the proton and neutron respectively, p – number of protons, n – number of neutrons.

The mass equation (20) does not involve the mass deficiency that, according to the Einstein equation $E=mc^2$, provides the binding energy between the nucleons. However, it allows to infer what is behind the origin of the nuclear forces. According to our hypothesis of the GR effect of field curvature in the space around the nucleus, we may define two zones as in the classical GR effect: a near zone close to the nucleus and a far zone. All our instruments detect the nuclear mass in the far zone. The only parameter that could serve as a scale etalon in Eq. (20) is the Compton wavelength, λ_C, and it is at a power of four. Consequently, it will mostly affect the nuclear mass m. In the near zone, λ_C should be shorter in comparison to our far zone. Similar to detection of the GR gravitational red shift of photons, our instruments will detect lower mass since our reference etalon λ_C (outside of the nuclear field curvature) is larger.

The above analysis leads to two important conclusions:

(1) The source of nuclear binding energy is the Static energy of the physical vacuum;
(2) The mass deficiency is a result of a GR effect of field micro-curvature around the atomic nucleus;

These conclusions allow us to explain how the nuclear energy is accessible. As in the macro field curvature, the strength of the field curvature around the atomic nucleus depends on the accumulated superdense mass. If the micro-curvature is changed due to fusion or fission, we will get a change in the atomic mass according to Eq. (20), whose equivalent energy is given by the Einstein equation $E=mc^2$. This energy is significant because it is a direct access to the hidden Static energy of the physical vacuum given by Eq. (19). Since these processes in microscale

are very fast, the physical vacuum exhibits a stress reaction that causes a depletion or fusion of nuclei accompanied with particle and gamma radiation.

Conclusion: The nuclear energy released in the fusion and fission reactions is a result of sudden changes of the GR space micro-curvature around the newly fused or depleted nuclei.

2.13. Considerations for successful cold fusion

Analysis of successful experiments by using the nuclear models according to the BSM-SG theory unveils the physics of the fusion process in which the Coulomb barrier could be overcome. This leads to the following recommendations.

1. The process of nuclear fusion in LENR is more probable between a heavier and a light nucleus (proton or deuteron) with a suitable neutron to proton ratio of the heavier nucleus.
2. Knowledge of the real 3D configuration of the nuclei helps to estimate the possibility for deeper penetration of the smaller nucleus into the heavier one. It also allows finding common structural features between elements involved in successful fusion in prior art.
3. The heavier element must be in a solid state in a powder form in order to increase its active surface
4. A proper temperature of the powder substance is required
5. A proper pressure of the light element gas is a prerequisite for the nuclear fusion process. The applied pressure must also be combined with a pressure pulsation.
6. Optional use of acoustic cavitation in a liquid phase.
7. Optional use of a plasma arc.
8. Optional use of a strong EM pulse with a broadband spectrum
9. Optional use of Tesla technology
10. Using a small amount of radioactive material

Consideration 1: The smaller nucleus has a shorter range of SG field than a larger nucleus. Then the smaller nucleus in a gas state could more easily move closer to the larger nuclei (as a powder) by applying some momentum via pulsating pressure, an increase of the Brownian motion by temperature, or by ultrasound.

Consideration 2: Heavier nuclei with larger free valences are not recommended since the valence protons (deuterons) have a larger angular freedom, expanding the Coulomb barrier, especially in the ionized state. Elements with smaller valences must be used. They are usually metals.

Consideration: 3. The active surface of the heavier element in solid state is increased a thousand times if it is in a micro-powder form. This also gives a room for realization of ion-electron pairs with their features described in §2.4.4. The reactor temperature must be kept below the melting point of the element.

Consideration 4: The heating increases the Brownian motion of the gaseous component and consequently increases the probability that the lighter nuclei will move closer to the heavier nuclei of the powder. The heavier nuclei may be considered as stationary while their vibrations increase with temperature.

Considerations 5: The constant pressure allows a deeper penetration of the lighter nuclei in the micro-powder, while the pulsating pressure might be helpful for homogenizing the mixture.

Consideration 6: The ultrasound in a liquid phase causes a cavitation with the effect of sonoluminescence or even sono-fusion. In fact, it invokes shock waves that may affect the Coulomb barrier (discussed later).

Consideration 7. The plasma arc is a complex process, involving different modes of plasma activations. In some kind of plasma excitations, the SG field in proximity to the nucleus might be directly affected that may invoke nuclear transmutation. Other specific modes are the Heterodyne Resonance Mechanism and the Driving Momentum of ion-electron pair in combination with the nuclear magnetic moment of the recipient nucleus. Nuclear transmutations have been observed in a variety of experiments involving plasma. Some plasma arc experiments are done in liquids.

Consideration 8. A strong EM pulse invokes a shock wave in the operative medium. At the boundary between the solid and gas phase the shock wave causes a stress in which the SG forces might modify the Coulomb barrier.

Consideration 9. Longitudinal (scalar) waves predicted by Lord Kelvin and practically realized by Nikola Tesla. These non-EM waves, generated by Tesla technology, exhibit stronger penetration capability. When penetrated in a substance they convert to EM pulse with a broadband frequency spectrum.

Consideration 10. The small amount of radioactive material could be used as a catalyzer. It is not necessary to be an alpha emitter. A material that provides beta particles is more suitable since it will not lead to radioactive waste by fission reactions if the heavier primary isotope is properly selected. The beta particles are specific high-energy waves that can trigger the formation of ion-electron pairs.

3. ANALYSIS OF COLD FUSION EXPERIMENTS BY USING THE BSM-SG MODELS OF ATOMIC NUCLEI

3.1 Theoretical considerations about using the BSM-SG models of the atomic nuclear structures

The BSM-SG models for the most abundant isotopes of the elements of the Periodic Table for $1 \le Z \le 103$ (Z – number of protons) are given in the Atlas of Atomic Nuclear Structures (ANS) [12]. It is included as an appendix to the BSM-SG book [4,13] and was also published elsewhere. Detailed description of the nuclear structures and how the nucleons are connected by different bonds is provided in Chapter 8 of the BSM-SG book. Part I of ANS (page 1-1 to page 1-4) shows the structure of the stable elementary particles: electron, proton and neutron with their physical dimensions and the nuclei of the simplest elements: Hydrogen, Deuterium and Helium. Part II of ANS (pages II-0 to II-20) shows the arrangement of nucleons (protons and neutrons) in the atomic nuclei for the stable isotopes of elements from Hydrogen to Lawrencium. The protons and neutrons comprising the atomic nuclei are connected by different types of bonds, as they are described in Chapter 8 of BSM-SG. In order to simplify the drawings in the Atlas of ANS, the shapes of protons and neutrons are drawn by symbols – an arrow for the proton and a cross-line for the neutron. The different bonds are also shown by symbols. In part II the nuclear structure of all elements are shown by two graphical views using the symbols. They show all the features of the real 3D nuclear structure of the elements, with the exception of its slight twisting. The latter feature is a result of the real shape of the proton that is not a flat curve but a 3D curve obtained by twisting a torus to a shape close to a figure 8. The electron orbits are not shown but they are easily identifiable, since their trajectory is defined by the close proximity shape of the proton's electrical field. For a clearer visualization of the nuclear shape, some selected atomic nuclei are shown on page II-21 in the Appendix ANS of BSM-SG book and Fig. 2 of this article. In this visualization, the nuclei are shown by two views: a polar view and a polar section.

3.2. Analysis of cold fusion experiments that use acoustic cavitation or strong EM pulse

One of the earliest researchers on cold fusion is Hugh. G Flyn (1913-1997), a former professor at the University of Rochester and a recognized expert on ultrasonic waves in liquids. In his patent "Method of Generating Energy by Acoustically Induced Cavitation Fusion and Reactor Therefore", granted in 1982 [27] he advised using the ultrasonic method for generating a bubble in a liquid metal or alloy injected with hydrogen isotopes (hydrogen or deuterium or tritium), and the application of a positive pressure on the bubble to accelerate the adiabatic stage which causes the bubble to contract to a smaller radius. At or near its minimum radius, the bubble generates a very intense shock wave. This causes hydrogen isotopes injected in the metal liquid to undergo thermonuclear reactions. Flyn suggests a method comprising a properly design reactor with correctly selected metals and alloys and operational parameters. One of the optimal choices for obtaining an energy output on the order of 200 KW is to use Li at a temperature of 1000K to 1200K (727C to 927C) in which a fusion of deuterium will start from the beginning. Flyn claimed that the proposed method creates a number of H – isotopes including Tritium and even Helium. One of the most energetic nuclear reactions claimed by Flyn is

$$ {}_1H^1 + {}_3Li^7 = 2\,{}_2H^4 + 17.35MeV \qquad (21) $$

The cold fusion theorist and Nobel Laureate Julian Schwinger in his talk at MIT on November

11, 1991 emphasized the cavitation method of cold fusion and associated it with a coherent sonoluminescence [28]. Mentioning the formation of tritium and helium by Flyn, Schwinger says: "*When I first heard about coherent SL (sono-luminescence), some months ago, my immediate reaction was: "This is a dynamical Casimir effect*". His statement is in full agreement with the BSM-SG concept, according to which the Casimir forces are signature of the SG forces. In a micro-scale range they are able to modify the Coulomb field.

Recently the cavitation method was brought to attention by some groups, and in 2006 R. P. Taleyarkhan and colleagues from Purdue University published an article in PRL about a laboratory sono-fusion experiment that invoked nuclear reactions by cavitation in a cell containing a deuterated benzene and acetone mixture [29].

Some cold fusion researchers claim that they obtained fission products by applying a strong EM pulse in a plasma environment. One of the prominent scientists and researchers using a plasma method for cold fusion is Ruggero M. Santilli. He developed a method that he named "spin coupling" as a pre-conditioning for cold fusion [30]. The preconditioned gas he called magnegas and the atoms – magnecules. Santilli built hadronic generators in which he used carbon and conveyed hydrogen or deuterium gas under pressure, and an electrical arc (plasma). He claimed that he observed excess heat from a fusion reaction (C + D -> N + energy). He says that the energy yield is larger if the gas is preconditioned as a "magnegas". According to BSM-SG, the Santilli magnecule of hydrogen (deuterium) corresponds to the ortho-state of the hydrogen (deuterium) molecule illustrated in Fig. 9.a. In a normal hydrogen gas, the molecules in such a state are a small percentage. The other para-state (Fig. 9.b) is more abundant since the molecular binding is stronger so it is more resistant to collision depletion due to Brownian motion. The application of plasma discharge may convert the para to the ortho–state. The two protons in H_2 ortho-state (Fig. 9. a.) (or deuterons for D_2 ortho-state) have an orientation similar to the two deuterons in the atomic nucleus of Gd, (Fig. 6.) that fuse into a He nucleus (alpha particle) at room temperature. Consequently, the ortho-state of the H_2, and especially the D_2 molecule, is more promising for cold fusion. This is illustrated in the next sections.

According to BSM-SG, a shock wave is created in both methods - the cavitation bubble fusion and the strong EM pulse in plasma. It involves stress at the boundary between the atoms of heavier and lighter elements. In such stress, the SG forces are directly accessed causing modification of the Coulomb barrier

Fig. 14 illustrates graphically (by BSM-SG atomic models) some of the reactions claimed by the group of Taleyarkham [29] and the reaction (21) suggested by Flyn. The process in the reaction (21) is shown in Fig. 14.c, where the $_3Li^7$ nucleus is comprised of He and T nuclei attached by GBpa bonds (§8.3.6, Chapter 8 of BSM-SG). The arrow symbol with *p* denotes a probability for the nuclear reaction. The nucleus of helium is shown by the symbol used in ANS. In the proton to neutron conversion the far field of the positive charge is emitted as a Beta particle (not shown), which is a virtual charge distinguished from the real positron. The real positron possesses a material helical structure – (structure 2 in Fig. 8).

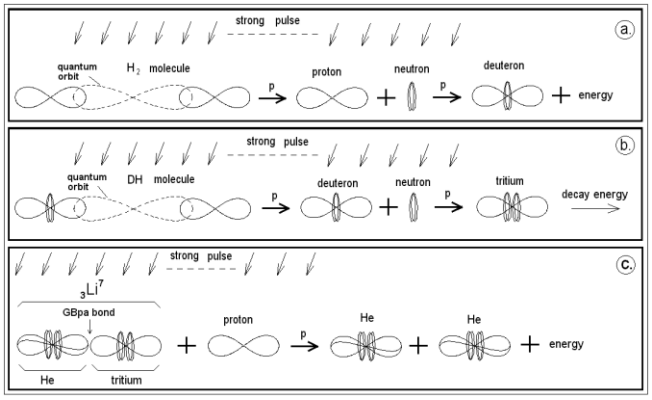

Fig. 14. Cold fusion by strong shock pulse in sono-fusion or EM pulse in plasma (a) H_2 -> p + n -> D; (b) HD -> D + n -> T, (c) L + p -> 2 He

Now let us focus on experiments based on Palladium and Deuterium in which a change of the natural isotope ratio Ag/Pd is observed. This means that a nuclear reaction Pd + D -> Ag takes place. Such results have been reported by Dash, J. and S. Miguet in 1996 [31]. The symbolic graphics of the nuclear structures of Pd and Ag are shown in the ANS Appendix A in BSM-SG book [18] and elsewhere [12].

The two views of Pd and Ag made from the symbolic graphics are shown in Fig. 15 together with the atomic nucleus of deuterium. The nuclear size dimensions are based on the dimensions of the proton, obtained in BSM-SG. The nuclear Coulomb barrier shown by a gray color is for illustration only (not based on calculations).

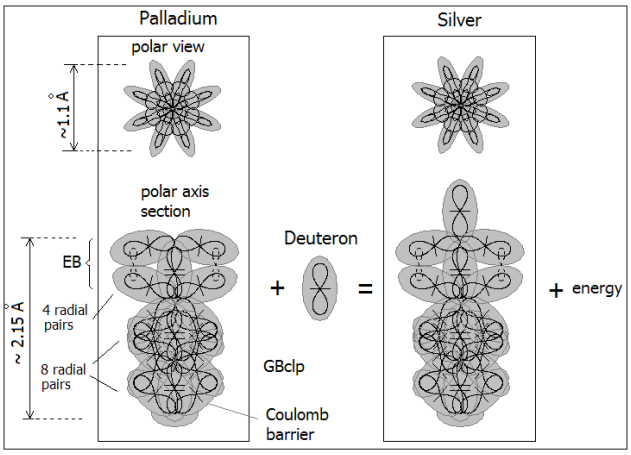

Fig. 15. Illustration of Pd+ D -> Ag reaction. The Coulomb barrier is shown by a gray color

It is apparent that a single deuteron is probably fused in the upper polar region of Pd converting it to Ag. What is the reason for expecting this to occur at the top pole? The answer will come from examining the trend of the atomic nuclear build-up with the z-number increase. The top pole contains four radial pairs of EB bonded deuterons, while the bottom pole contains 8 pairs of GBclp bonded deuterons. The upper Coulomb barrier at the top pole is more rarefied and the single deuteron may penetrate closer. The four pairs of deuterons are connected by quantum orbits, so they are called Electronic Bonds (EB). The EB bonds are excluded from the principal valence, but they could be broken in some strong chemical reagents. The single deuteron at the top pole in silver defines the principal valence. Or, it could be a proton only. The GBclp (close proximity gravitational bonds) are superstrong since they are held by SG forces. These bonds make the completion of the shells at noble gases so they are completely excluded from any valence. The middle section of the nuclear chain also contains 8 radial pairs of GBclp but they are slightly squeezed by the SG forces to make the nucleus more compact (this becomes clearer when the whole 3D nuclear structure is rotated). The middle and bottom region of 16 deuterons corresponds to the completed internal shell of the electrons according to the QM models. Some pairs can be from tritium nuclei.

In the hot fission or fusion experiments, the nuclear reaction is always accompanied by radioactivity and especially alpha radiation. The alpha particles are helium nuclei. One of the objections against cold fusion was that helium is not detected, but this is not true. Dr. Les Case from New Hampshire is one of the first who detected helium using palladium as a catalyst in a deuterium atmosphere. This phenomenon, called "Case effect", has been confirmed by other researchers [32]. The palladium in this case of nuclear reaction plays the role of a catalyst. The process is illustrated in Fig. 16 by using the BSM-SG nuclear models.

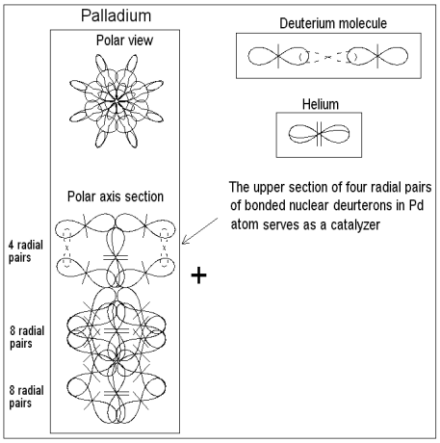

Fig. 16. The role of Palladium as a catalyst for the nuclear reaction D+D -> He from the point of view of the BSM-SG theory

The deuterium molecule D_2 in its most common state is similar to the H_2 molecule shown in Fig. 9.a. (analysis for the D_2 is made in §9.8, Chapter 9 of BSM-SG). In order to fuse to helium, the following two conditions are necessary:

(1) The two deuterons must get much closer, while keeping the axial orientation (as in the case of deuterons preceding the alpha decay in Gd, shown in Fig 6),

(2) The Coulomb barrier of the proton shown in Fig. 4 must be temporarily disturbed. These conditions could be fulfilled if the D_2 molecule is pushed and temporarily trapped between the 4 deuteron pairs at the upper pole region of the Pd nucleus. At room temperature and normal

pressure, such a process has a low probability. However, if applying Considerations 3, 4, and 5, the probability may increase, leading also to an increase of the energy yield.

3.3 Advances in cold fusion research in Italy.

The research on cold fusion in Italy was initiated in 1989 by Francesco Piantelli, a professor at the University of Sienna. He observed a strange thermal effect at low temperature in a sample of nickel in hydrogen atmosphere. Piantelli has a few patents and publications [4]. He designed reactors and did extensive research on different elements in hydrogen and deuterium atmosphere and obtained fusion byproducts and energy release**.** He used mostly rods coated with the selected elements by special technology. The research of Piantelli was extended and supported by the local inter-university centers from Bologna (Focardi, Campari) and Sienna (Piantelli, Gabbani, Montalbano, Veronesi). A detailed report about this research is published by the Italian National Agency for New Technology, Energy and Environment in 2008 [5]. The nuclear process suggested by Pinatelli is

$$Ni + H \rightarrow Cu \quad or \quad Ni + D \rightarrow Cu. \qquad (22)$$

Fig. 17 illustrates the reaction Ni + D-> Cu by using the BSM-SG models. Comparing the atomic nucleus of Ni (Fig. 17) with the nucleus of Pd (Fig. 16) we see some similarity in their configuration. The upper polar regions for both nuclei contain 4 radial pairs of Deuterons. Consequently the reaction Ni + D -> Cu becomes similar to the reaction Pd + D -> Ag.

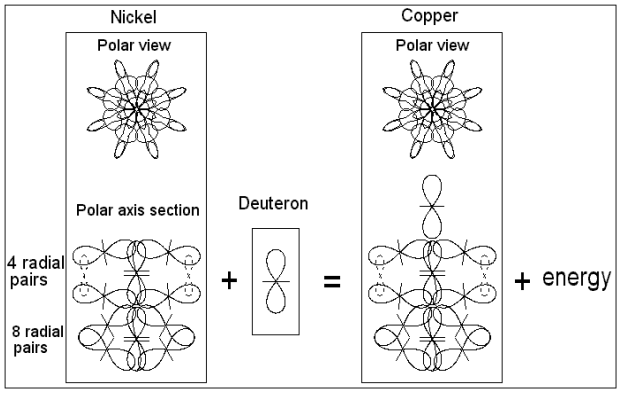

Fig. 17. The nuclear reaction Ni + D -> Cu illustrated by BSM-SG models

The method of Piantelli has been further elaborated by Sergio Focardi, an emeritus professor at the University of Bologna and Andrea Rossi, an inventor and entrepreneur [6]. This led to the development of a commercial prototype of reactor by Rossi with significant output energy in order of kilowatts, where the main expected fusion reaction is Ni + H -> Cu. Andrea Rossi filed a patent application on April 9, 2008 [7].

On January 14, 2011, Rossi and Focardi gave the first public demonstration announcing that the reactor called E-cat is capable of producing about 5 to 10 kilowatts of heat power, while only consuming a fraction of that. During the year 2011, five additional demonstrations and tests were provided. On October 28, 2011, Rossi demonstrated 1 MW system comprised of 56 parallel reactors. According to Rossi, the system working with a reduced power for safety produced total heat energy of 2635 KWH for five hours.

According to our analysis, the major success of cold fusion implemented in the E-cat reactor is due to the following improvements over the prior art. The first one is that Nickel is in the form of powder with an average granular size of about 10 um, obtained via some private technology. The second one is that a pulsing pressure is superimposed on a highly pressurized hydrogen gas. The first one matches our consideration (3), while the second one matches the consideration (5). The other considerations (1) and (4) are also applied in the E-cat reactor, while consideration (2) might have been intuitively guessed by Piantelli since Nickel is in the same vertical group as Palladium. Some public reports mentioned that an RF generator was used, but it might only have helped to initiate the cold fusion reaction. Also, it may not be a standard RF generator, but a generator providing a burst of frequencies.

According to Rossi, he also uses a catalyzer based on a small number of elements. We may speculate that Rossi probably introduced a small quantity of beta radioactive elements. This helps to creation of ion-electron pairs of hydrogen (Rydberg atoms) that in combination of a proper nuclear spin state of Ni might facilitate the nuclear fusion. This effect is discussed in the book “Structural Physics of Nuclear Fusion” [24].

Rossi claimed that he obtained successful results when using the isotopes Ni^{62} and Ni^{64} (34 and 36 neutrons). The expected reactions are:

$$Ni^{62} + H \rightarrow Cu^{63} + 5.622\ MeV \quad (23)$$

$$Ni^{64} + H \rightarrow Cu^{65} + 6.945\ MeV \quad (24)$$

All involved elements in the above two reactions are stable isotopes. A small amount of Zn was also detected, as this is evident from Fig. 3 and Fig. 4 of Rossi's patent application [14]. It is interesting to point out that for experiments involving these two reactions, no radioactive byproducts or hard radiation has been detected with the exception of some low energy X-rays. Only insignificant amounts of some fission byproducts have been detected as shown in [14].

If using Ni isotopes with lower numbers of neutrons or Ni^{63}, the obtained copper isotope is not stable and it decays. As well, such reactions are obviously not preferred due to creation of some radioactivity. The preferable reactions according to Focardi and Rossi are (3.9) and (3.10) in which the nuclear energy is released as heat. In both reactions, according to BSM-SG models, the proton is captured by the nickel nucleus, converting it to copper. The group of Defkalion research on the reaction Ni + H also claims traces mainly of copper and zinc [35].

Fig. 18. illustrates the nuclear structures of Ni, Cu and Zn according to the BSM-SG models.

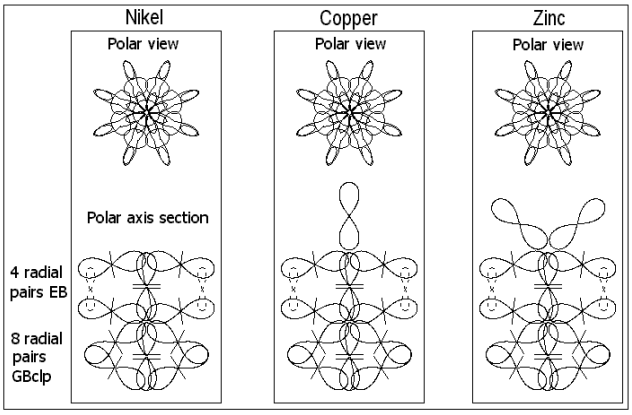

Fig. 18. Ni, Cu and Zi nuclei. Ni nucleus is embedded unchanged in Cu and Zn nuclei. The single unbound proton in Cu and the two unbound protons in Zn define their principal valence.

According to BSM-SG, the stable isotopes of Ni with a larger and even number of neutrons have four pairs in the upper polar region that are more likely deuterons or tritiums nuclei rather than protons. In this case the Coulomb barriers are more compact, allowing closer penetration of the proton or deuteron from the gas. The tritium nuclei, although stable in the nucleus, could decay more easily by releasing a neutron, if disturbed. This may cause some fission reactions that could explain the small amounts of lighter elements detected (such as sulfur, chloride, potassium, calcium) after operation of the E-cat reactor.

3.4. Cold fusion advances by other groups and researchers.

The plasma effect is used also by a number of individual researchers and researchers groups, such as M. Kanarev [19], R. Santilli [30], George Egely [33], Emanuele Costa [34], Defkalion group [35] and many others. Another method suggested by F. Celani also gets international attention [36]. As a result, an initiative was established in 2012 as an open project called Quantum Heat with a head quoter in USA [37].

Defkalion researchers used also nickel in a micropowder form (maybe not the same isotopes as Focardi and Rossi) and hydrogen under pressure. They, however, introduced a plasma discharge in their Hyperion rector. In their article presented at the at the ICCF 17 conference in S. Korea, 2012, they say [35]: *In Hyperion reactors the atomic H has to be "excited" to its Rydberg state. Its electron's trajectory becomes elliptic, so the atom behaves like a dipole. Such dipoles can be polarized and "guided" to a target. At first, we introduced the plasma ignition method (DC pulsed at 24KV/22 mA at some KHz) to produce glow discharges in a high pressure (2-8 bar) hydrogen envelope, by use of specially shaped tungsten and TZM electrodes, resulting in the above.*

According to our analysis of Defkalion method the Rydberg atoms are ion-electron pairs involved in a mechanism discussed in [24]. The plasma discharge might provide not only condition for generating of such pairs but also a spin change of the nickel nuclei. At proper spin state the magnetic field of the ion-electron pairs (dominated by the large magnetic moment of the electron) and the magnetic field of the nickel nucleus interact complimentary that may assist the overcoming the Coulomb barrier of the nucleus of nickel. This

theoretically predicted effect is discussed in [24]. This is according to consideration (7).

3.4. Prediction for other cold fusion reaction

It is worth noting that, based on our analysis of the successful cold fusion processes, we conclude that another option of cold fusion based on Cr instead of Ni could be also feasible. Fig. 19. illustrates the nuclei of Cr, Mn and Fe using the BSM-SG models. The chromium nucleus has some similarity to the nucleus of nickel with the only difference that it has 2 radial pairs with EB bonds in the upper polar region instead of 4 pairs in nickel.

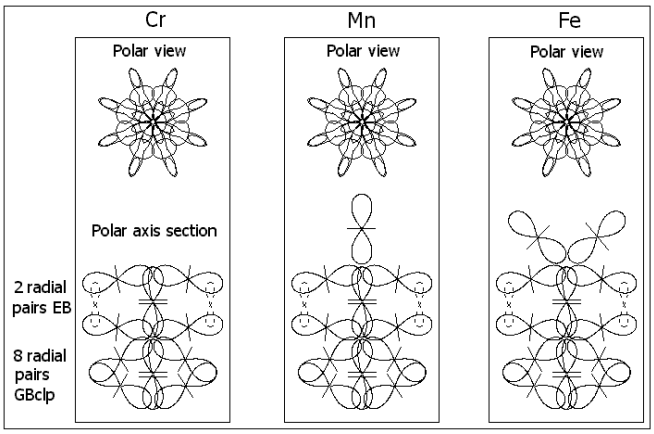

Fig. 19. Cr, Mn and Fe nuclei according to the BSM-SG models

The similarity is apparent from the similarity between the Lamb shift patterns of the group of Cr, Mn and Fe and the group of Ni, Cu, and Zn shown in Fig 13.a. and also from other considerations discussed in Chapter 8 of BSM-SG.

The predicted reactions are:

$$Cr^{54} + H \rightarrow Mn^{55} + 7.559\ MeV \qquad (25)$$

$$Cr^{52} + H \rightarrow Mn^{53} + 6.052\ MeV \qquad (26)$$

The isotopes Cr^{52}, Cr^{54}, Mn^{53}, Mn^{55} are stable isotopes, but Mn^{53} is a traceable i. e. its natural abundance is insignificant. The predicted reaction (25) should not lead to radioactive byproducts. It may require higher activation temperature in comparison to reactions (32) and (24). The predicted reaction (26) is useful as a signature that the applied technical method leads to cold fusion. This is so because the output of reaction (26) is a traceable isotope.

4. DISCUSSIONS AND CONCLUSIONS:

The structural physical models of atomic nuclei suggested by the BSM-SG theory provide a new view about nuclear reactions and, more particularly, the feasibility of cold fusion. The Coulomb field below the Bohr radius does not converge to a sphere with a radius of about 1×10^{-15} (m) and it is also not spherical. So the Coulomb barrier of the proton does not rise to a very high strength. The Coulomb barrier of the atomic nucleus is formed from superimposed Coulomb barriers of the protons as illustrated in Fig. 15. The shape of the nuclear Coulomb barrier might be slightly modified from the neighboring atoms in solids and especially in a metal lattice. It could also be affected by some technical methods that cause a stress. Additionally, a physical effect of ion-electron driving momentum in combination with a proper spin state of the recipient nucleus might help overcoming the Coulomb barrier. The predicted effect is described in [24]. [The practical considerations in section 2.13 suggest a selection of isotopes and methods that may lead to successful cold fusion reactions without radioactive byproducts. The nuclear structures presented in the ANS provide information for selection of the involved elements. From the point of view of the BSM-SG nuclear models, the lack of radioactive byproducts and the insignificant amount of radioactivity in cold fusion experiments is reasonable, because the nucleus of the recipient element is not severe disturbed like in the nuclear fission chain reactions. The major advantages of cold fusion over the nuclear reactors based on chain fission reaction are the smooth release of energy and the lack of radioactive byproducts or strong radioactivity.

ACKNOWLEGMENTS:

This essay is based upon private work partially supported by the World Institute for Scientific Exploration. Any opinions, conclusions or recommendations expressed in this material are those of the author and do not necessarily reflect the official view of the scientific institution employing the author.

REFERENCES:

1. M. Fleischmann and S. J. Pons, Electroanal. Chem, **261**, 301, (1989)
2. http://www.lenr-canr.org/ Low energy nuclear reaction (LENR) or cold fusion; http://www.iscmns.org/ International Society for Condensed Matter Nuclear Science
3. E. F. Mallove, Universal Appeal for Support, (open letter), http://merlib.org/node/5629
4. Francesco Piantelli, Energy generation and generator by means of anharmonic stimulated fusion, Patent WO 9520816 (1997).
5. Cold Fusion. The history of research in Italy. Italian National Agency for New Technologies, Energy and Environment, 2008 http://old.enea.it/com/ingl/New_ingl/publications/pdf/Cold_Fusion_Italy.pdf also: Asti Workshop on Anomalies in Hydrogen Deuterium loaded Metals, Infinite energy, Dec-Jan 1998 (#17), 1-9.
6. S. Focardi and A. Rossi, http://www.journal-of-nuclear-physics.com/?p=360
7. A. Rossi, Method and Apparatus for Carying out Niclkel and Hydrogen Exothermal Reactions, WO 2009/125444 A1 (15 Oct 2009) (patent submitted 4 Aug 2008).
8. NASA LENR conference, September 22, 2011. http://www.scribd.com/doc/75267974/NASA-Langley-Zawodny-GRC-LENR-Workshop
9. S. Sarg. Helical Structures Forum http://www.helical-structures.org (launched on 17 Oct 2011)
10. S. Sarg, *New vision about a controllable fusion reaction*, monograph, www.nlc-bnc.ca/amicus/index-e.html (ISBN 0973051523, April, 2002), (AMICUS No. 27276360); Canadiana: 20020075960
11. S. Sarg ©2001, *Basic Structures of Matter*, monograph, http://www.nlc-bnc.ca/amicus/index-e.html (First edition, ISBN 0973051507, 2002; Second edition, ISBN 0973051558, 2005), (AMICUS No. 27105955), LC Class no.: QC794.6*; Dewey: 530.14/2 21
12. S. Sarg © 2001, Atlas of Atomic Nuclear Structures, ISBN 0973051515, http://www.nlc-bnc.ca/amicus/index-e.html (April, 2002), (AMICUS No. 27106037); Canadiana: 2002007655X, LC Class: QC794.6*; Dewey: 530.14/2 21 (also http://vixra.org/abs/1107.0031)
13. S. Sarg, New approach for building of unified theory, http://lanl.arxiv.org/abs/physics/0205052 (May 2002)
14. Sarg, A Physical Model of the Electron according to the Basic Structures of Matter Hypothesis, Physics Essays, vol. 16 No. 2, 180-195, (2003) http://physicsessays.org/doi/abs/10.4006/1.3025574
15. S. Sag, BSM theory and derived atomic models, www.journaloftheoretics.com/Links/Papers/Sarg.pdf
16. S. Sarg, BSM - Supergravitation unified theory based on an alternative concept of the physical vacuum, Proceedings of the IX International Scientific Conference "Matter, Energy, Gravitation", 7-11 Aug 2006, St. Petersburg, Russia.
17. Basic Structures of Matter – Supergravitation Unified Theory based on an Alternative Concept of the Physical Vacuum, Proceedings of Natural Philosophy Alliance, 17th Annual Conference 23-26 July, 2010, Long Beaches, CA
18. Stoyan Sarg, *Basic Structures of Matter – Supergravitation Unified Theory*, Trafford Publishing, 2006, ISBN 1412083877 Book review in Physics in Canada http://www.cap.ca/brms/Reviews/Rev813_486.pdf
19. Ph. M. Kanarev, and Tadahiko Mizuno, Cold fusion by plasma electrolysis of water, http://guns.connect.fi/innoplaza/energy/story/Kanarev/coldfusion/index.html
20. Ph. M. Kanarev, Models of the Atomic Nuclei, http://www.journaloftheoretics.com/Links/Papers/Kanarev-Atomic.pdf
21. Image of carbon sheet, Popular Science, (01.19.2010) (Public data) www.popsci.com/gadgets/article/2010-01/graphene-breakthrough-could-usher-future-electronics
22. J. E. Polard et al, Journal of Chemical Physics, **77**, 34-46 (1982) (PE spectra)

23. I. Dabrowsky, Canadian Journal of Physics, **62**, 1639 - (1984) (H2 optical spectra)
24. Stoyan Sarg, *Structural Physics of Cold Fusion with BSM-SG Atomic Model*, (2013), ISBN 978-1482620030. Amazon.com.
25. G. W. Erickson, Energy Levels of One-Eelectron Atoms, Phys. Chem. Ref. Data, V.6, No. 3, (1977)
26. A. Einstein, *Sidelights on Relativity*, translated by: G. B. Jeffery and W. Perret, Methuen & Co. London, (1922); republished unabridged and unaltered: Dover, New York, (1983)
27. H. G. Flyn, Method of generating energy by acoustically induced cavitation fusion and reactor therefore, US Patent 4,333,796 (filed 1978, issued 1982)
28. J. Schwinger, A progress Report: Energy Transfer in Cold Fusion and Sonoluminecsence, Infinite Energy, Issue 24, p. 19, (1999)
29. R. P. Taleyarkhan et al., Modeling, analysis and prediction of neutron emission spectra from acoustic cavitation bubble fusion experiments, Nuclear Engineering and Design, 238, 2779-27-91, (2008)
30. R. Santilli http://santilli-foundation.org/
31. Dash, J. & S. Miguet, *Microanalysis of Pd Cathodes after Electrolysis in Aqueous Acids.* J. New Energy, **1**(1): 23, 1996.
32. Case effect observed by Dr. Les Case from New Hampshire http://pages.csam.montclair.edu/~kowalski/cf/47catalytic.html
33. G. Egerly, Nano Dust Fusion, Infinite Energy, March/april 2012, Issue 102, 11-23
34. Emanuele Costa, Private com.
35. http://newenergytimes.com/v2/conferences/2012/ICCF17/ICCF-17-Hadjichristos-Technical-Characteristics-Paper.pdf
36. F. Celani et al, Development of a High Temperature Hybrid CMNS Reactor, www.ilperiodico.it/pdf/fusione_fredda.pdf
37. Open project Quantum Heat www.quantumheat.org

About the author.

Stoyan Sarg - Sargoytchev, a Bulgarian born Canadian, holds engineering diploma and PhD in Physics. From 1976 to 1990 he worked on space projects coordinated by the program Intercosmos, established by the former Soviet Union in collaboration with European countries. From 1990 he was a visiting scientist of Cornel University for two years and worked at Arecibo Observatory, PR. At the end of 1991 he immigrated to Canada where he took scientific positions with different institutions: University of Western Ontario, Institute for Space and Terrestrial Research and currently with York University. Paying attention on unsolved problems in Physics he arrived to original idea about structural physical models of elementary particles and atomic nuclei. His treatise "Basic Structures of Matter - Supergravitation Unified Theory" (BSM-SG) was firstly archived in NLC of Canada in 2002 and published as a book in 2006. Related articles were published in scientific journals, physical archives and proceedings of conferences. Presently, Stoyan Sarg is an emeritus member of the Society for Scientific Exploration and a Distinguished scientific advisor at the World Institute for Scientific Exploration.

http://instituteforscientificexploration.org/